Broad-band and Omnidirectional Antireflection Coatings Based on Semiconductor Nanorods

By *Silke L. Diedenhofen,* Gabriele Vecchi, Rienk E. Algra, Alex Hartsuiker, Otto L. Muskens, George Immink, Erik P. A. M. Bakkers, Willem L. Vos,* and *Jaime Gómez Rivas*

Over the last years, there has been an increasing interest in reducing the reflection of surfaces by fabricating antireflection coatings.[1–16] Antireflection coatings can be applied to minimize the reflection for optical components,[4] to improve the light coupling into solar cells,[5] or to enhance the extraction of light from light-emitting diodes (LEDs).[6] Depending on the structure of the antireflection layers, these can be classified into two types, namely antireflection coatings composed of i) homogeneous layers and ii) inhomogeneous layers.[15] Homogeneous antireflection coatings, or step-index coatings, reduce the reflection by destructive interference of light reflected at different interfaces. For these coatings, the material and thickness of the layer have to be chosen carefully for each wavelength, angle, and substrate. The bandwidth of these coatings is lower than one octave, for example, 400–700 nm or 800–1100 nm, and the angle of incidence is limited to 30 °.[16] The other type of antireflection coatings, or the inhomogeneous layers, form the so-called graded index coatings. They are advantageous over step index coatings with respect to omnidirectionality and broad-band behavior. Theoretically, a drastic reduction of the reflection for angles up to 80 ° and for a wavelength range of one order of magnitude is shown, for example, from 400 nm to 4 μm.[3] In this kind of coating, the refractive index is gradually increased from that of the surrounding material to the refractive index of the substrate, and the reflection is decreased by optical impedance matching at the interfaces. Figure 1a shows a schematic representation of the reflection of a substrate with a homogeneous and graded index coating.

The fabrication of graded index coatings is very challenging when the substrate is surrounded by air, as a solid material that matches a refractive index of 1 is needed. Obviously, the refractive index of any dense solid material is too large to match the refractive index of air. To overcome this problem, more effort has been made over the last years to obtain graded index coatings, by applying nanostructuring techniques inspired by biological structures such as moth eyes.[17,18] With these techniques, it is possible to fabricate layers of porous materials that have an effective refractive index close to 1 on the upper part and a larger index at the bottom. Recently, a graded-refractive-index structure was fabricated in a bottom–up process using SiO_2 and TiO_2 nanorods deposited on AlN.[7] Using this technique, a graded index is achieved by varying the filling fraction from one layer to the next, and by changing the material from a low-index material at the top (SiO_2) to a material with a higher refractive index at the bottom (TiO_2). Therefore, the evaporation of two materials is necessary for these coatings. A different bottom–up approach based on chemical vapor deposition has led to recent demonstrations of antireflection coatings consisting of single materials.[5] These coatings are formed by ZnO nanowires grown on a Si substrate. The use of silicon substrates in Ref. [5] did not allow transmission measurements for visible wavelengths, and the effects of light scattering by the nanowires on the reduction of the reflection could not be determined. With top–down nanostructuring processes, the reflection of Si has been reduced by etching different kinds of nanostructures into the substrate.[8–11] With these etching techniques, very low values of the zeroth-order or specular reflection have been reported. However, it has not been clearly stated whether this reduced reflection occurs due to light scattering by the nanostructures, to an enhanced absorption in the antireflection layer, to refractive index matching to the substrate, or to a combination of these phenomena. An important limitation of etched silicon surfaces is that the

[*] S. L. Diedenhofen, Dr. G. Vecchi, Dr. J. Gómez Rivas
FOM Institute for Atomic and Molecular Physics
c/o Philips Research Laboratories
High Tech Campus 4
5656 AE Eindhoven (The Netherlands)
E-mail: diedenhofen@amolf.nl
R. E. Algra
c/o Philips Research Laboratories, High Tech Campus 4
5656 AE Eindhoven (The Netherlands)
R. E. Algra
Materials Innovation Institute (M2i)
2628 CD Delft (The Netherlands)
R. E. Algra
Department of Solid State Chemistry
Institute for Molecules and Materials (IMM)
Radboud University
Toernooiveld 1, 6525 ED Nijmegen (The Netherlands)
A. Hartsuiker, Dr. O. L. Muskens
FOM Institute for Atomic and Molecular Physics
Kruislaan 407, 1098 SJ Amsterdam (The Netherlands)
G. Immink
Miplaza Technology Laboratories
Philips Research Europe
High Tech Campus 29, 5656 AE Eindhoven (The Netherlands)
Dr. E. P. A. M. Bakkers
Philips Research Laboratories, High Tech Campus 4
5656 AE Eindhoven (The Netherlands)
Prof. W. L. Vos
FOM Institute for Atomic and Molecular Physics
Kruislaan 407, 1098 SJ Amsterdam (The Netherlands)
Prof. W. L. Vos
Complex Photonic Systems,
MESA+ Institute for Nanotechnology, University of Twente
7500 AE Enschede (The Netherlands)

DOI: 10.1002/adma.200802767

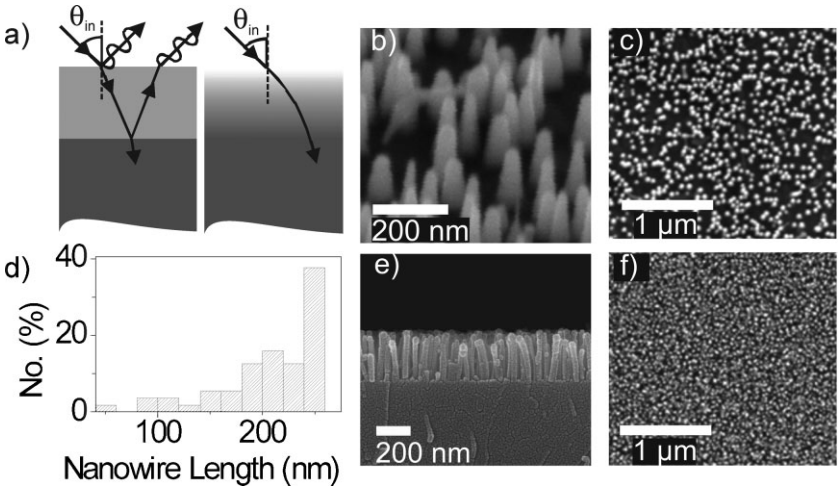

Figure 1. a) Schematic of the reflections of a substrate with a homogeneous (left) and a graded-refractive-index coating (right). The homogeneous coating reduces the reflection due to interference of light reflected at the air-coating layer and at the coating layer/substrate interfaces. For simplicity, just one reflection path is shown, which stands for the multiple reflections occurring at the interfaces. For the graded index coating, no reflection occurs, as the refractive index is matched at the top and bottom interfaces. b,c,e, and f) SEM images of nanorods. b) Image of conically shaped nanorods (sample I) tilted under 30° with respect to the normal of the sample. c) Top-view image of the same sample. e) Side-view image of cylindrical nanorods (sample II). f) Top-view image of the same sample. The SEM image in b) is magnified to show the tapering of the wires, and the image in e) shows more nanorods, to display the distribution in length of the rods. d) Length distribution of the nanorods in sample II.

antireflection layer is also absorbing. The fabrication of nonabsorbing antireflection layers on top of absorbing substrates is thus impossible by etching. It is also worth mentioning that ultralow reflection was recently reported for layers of carbon nanotubes.[12,13] This reduced reflection was mainly caused by absorption.

Here, we unambiguously demonstrate by measuring the transmission and reflection of GaP nanorods on top of a GaP substrate that the reduction of the reflection in these layers is mainly caused by a graded-refractive-index coating and interference in the nanorod film, and that the role of scattering losses and absorption by the nanorod layer is secondary. The broadband reduction of the reflection is demonstrated by zeroth-order or direct transmission and specular reflection measurements at wavelengths in the visible and near-infrared regions, and by angle-integrated total reflection and transmission measurements. To investigate the omnidirectionality of the antireflection coating, transmission and reflection measurements are performed for angles up to 60°. We have chosen to work with GaP nanorods on top of a GaP substrate as the electronic band gap of GaP is located at 548 nm, and transmission measurements are possible for the red and near-infrared parts of the spectrum. The investigated coatings of nanorods were fabricated in a bottom–up process using the vapor–liquid–solid (VLS)-growth mode[19] by chemical vapor deposition. In contrast to etching techniques, this technique allows the heteroepitaxial growth of several semiconductors of groups IV,[20,21] III/V,[22,23] and II/VI[5,24] on different substrates.[25]

We have investigated the antireflection properties of two types of nanorods, namely cylindrically and conically shaped rods. In ensembles of conically shaped nanorods, a graded refractive index can be achieved with a low effective refractive index at the top and a high effective index at the bottom, due to the variation of the filling fraction of GaP along the growth direction of the rods. The cylindrical nanorods show an antireflection behavior, due to a distribution of nanorod lengths that leads to a reduced density toward the top of the layer. The investigated coatings of nanorods were fabricated on a double-side polished GaP substrate with a thickness of 500 μm. On the backside of the substrate, a film of SiO_2 with a thickness of 500 nm was deposited, to avoid etching of this surface during a surface cleaning process before the growth. A more detailed description of the fabrication is given in the Experimental section. The growth can be controlled by adjusting the temperature of the substrate during growth, in such a way that either vertically aligned cylindrical nanorods or conically shaped nanorods can be fabricated. The initial diameter of the nanorods is determined by the size of gold particles used to catalyze the growth, and thus determines the diameter at the top of the rod. During the vertical growth of the nanorods, it is also possible to induce a side-wall growth, when the temperature exceeds the critical value.[26] For one of the samples investigated, which will be called sample I, the temperature was such that lateral growth is significant. The base of the nanorods is exposed to the side-wall growth for the longest time, the diameter is the largest at this position, and it gradually decreases toward the top of the rod. The apex angle of the conical shape can be tuned, as the lateral growth is more pronounced with respect to the vertical growth at higher temperatures.[26] The other sample, which will be called sample II, is grown at a lower temperature, where vertical growth is dominating, leading to nontapered vertically aligned rods.

Figure 1b and e shows scanning electron microscopy (SEM) images of samples I and II, respectively. The GaP filling fraction increases from the top to the bottom of the nanorod layer, due to tapering for sample I. For sample II, an increase in GaP filling fraction occurs because of the nanorod-length distribution. Figure 1c and f shows top-view SEM images of samples I and II, respectively. The density of nanorods for sample II is higher than for sample I, while the nanorods in sample I have a larger diameter at the bottom. The difference in density is due to different growth conditions for both samples (see Experimental section). As has been observed before, and we have confirmed with sample II, variations in rod density and diameter lead to a distribution in the lengths of the rods.[22] A histogram representing the length distribution of sample II is given in Figure 1d. This distribution was obtained by measuring the length of 56 nanorods from SEM images such as Figure 1e. The length of the rods varies from 50 to 250 nm, while the majority of rods have a length of 250 nm. The growth parameters and the characteristic dimensions for both samples are summarized in Table 1. To further verify the structure of the nanorods, Figure 2a and b shows transmission electron microscopy (TEM) images of

Table 1. Growth time and temperature of GaP nanorods. Sample I consists of conically shaped nanorods, while sample II is formed by cylindrical structures. The averaged nanorod length and diameter at the top and bottom part of the nanorods are also listed. These values were obtained from SEM images.

Sample	Growth time [s]	Growth temperature [°C]	Length [nm]	Top diameter [nm]	Bottom diameter [nm]
I	600	570	178 ± 25	28 ± 7	63 ± 9
II	320	420	208 ± 50	27 ± 5	27 ± 5

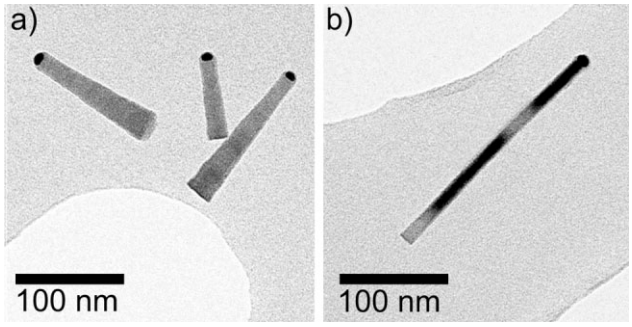

Figure 2. TEM images of a) conical nanorods (sample I) and b) cylindrical nanorods (sample II).

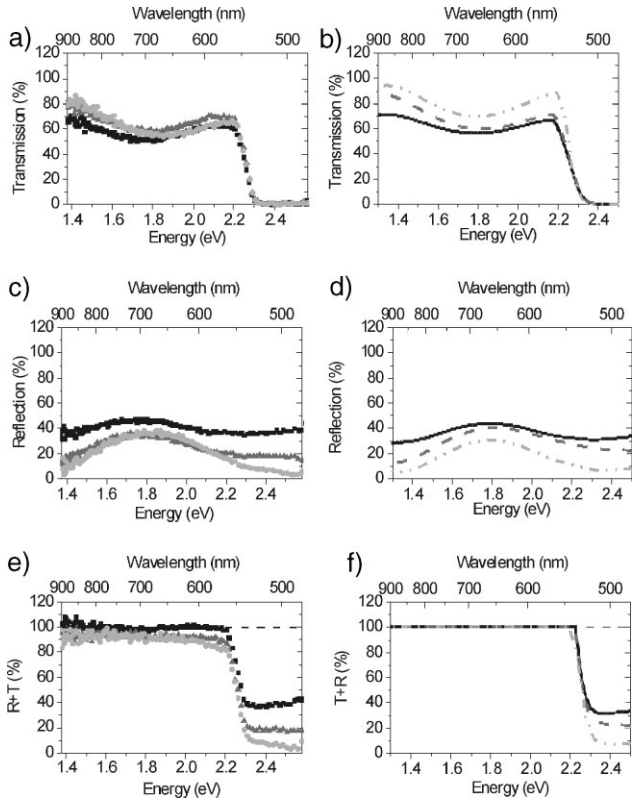

Figure 3. a) Measured transmission and b) calculated transmission for normal incidence, c) measured reflection and d) calculated reflection at an angle of incidence of 6°, e) the sum of measured reflection and transmission, and f) the sum of calculated reflection and transmission. The measurements (calculations) for a bare GaP substrate with one side covered by a 500 nm layer of SiO_2 are shown as black squares (black solid curve). The light-gray circles (light-gray dash-dot-dotted curve) and the dark-gray triangles (dark-gray dashed curve) correspond to the measurements (calculations) of sample I and II, respectively.

both types of rods. On all rods, the gold particle on top is visible. The darker and lighter regions of the rods are related to twinning defects.[27] These defects do not have a significant effect on the nanorod refractive index, and do not modify reflection characteristics of a nanorod layer.[27,28] These images show a clear difference between the conically shaped (Fig. 2a) and cylindrical (Fig. 2b) rods. For the conical rods, a tapering angle of around 3° can be estimated.

We have determined the broad-band specular reflection on and direct transmission through the samples using the setup explained in the Experimental section. The transmission was measured at normal incidence, while the reflection was measured at an angle of incidence of 6° with respect to the surface normal. The resulting transmission and reflection spectra are displayed in Figure 3a and c, respectively, with light-gray circles for sample I and dark-gray triangles for sample II. For comparison, we also plot the transmission and reflection measurements of a bare GaP substrate with 500 nm SiO_2 at the backside (black squares). The sharp absorption edge visible for all samples at 2.26 eV ($\lambda = 548$ nm) is due to the electronic band gap of GaP. The small dip in the transmission and the maximum in the reflection of the GaP substrate around 1.76 eV ($\lambda = 700$ nm) are due to a Fabry–Pérot resonance in the SiO_2 layer at the backside of the GaP substrate. The scattering losses of the samples can be estimated by adding the transmission and reflection measurements (see Fig. 3e). For the GaP substrate (black squares), the transmission plus reflection is 100% for energies below 2.26 eV; as expected, there are no losses in the measurement of the reference below the band gap in GaP. For higher energies, interband absorption has a dominant influence. For sample I, the transmission from around 1.88 eV ($\lambda = 660$ nm) to 2.3 eV (550 nm), is not increased with respect to the transmission of the bare GaP substrate. At these energies, Rayleigh scattering by the nanorods reduces slightly the transmission of sample I, cancelling the enhancement of this transmission due to the antireflection.[27] For lower energies, however, the transmission increases as scattering losses become negligible. At 1.38 eV ($\lambda = 900$ nm), the transmission of sample I is increased by 20% compared to the substrate. The small shift of the dip in transmission and the peak in reflection at around 1.85 eV (670 nm) compared to the transmission and reflection of the substrate is related to a Fabry–Pérot reflection in the nanorod layer, superimposed to the reflection in the back SiO_2 layer. The sum of reflection and transmission (Fig. 3e) for sample I (light-gray circles) increases from 85% at 2.15 eV ($\lambda = 575$ nm) to around 95% at 1.38 eV ($\lambda = 900$ nm). The small reduction of the sum of reflection and transmission when increasing the energy can be attributed to light scattering in the nanorod layer.

From the transmission measurement of sample II (dark-gray triangles in Fig. 3a), we can estimate an increase in the transmission of around 13% relative to the bare GaP substrate for energies below the electronic band gap. This nanorod antireflection coating consists of thinner nanorods than sample I (see

Table 1), so Rayleigh scattering is less pronounced in the range of wavelengths considered. For this sample, the sum of reflection and transmission (dark-gray triangles in Fig. 3e) shows a flat wavelength response of around 95%. The sum of reflection and transmission measured slightly lower than 100% can be assigned to residual scattering in the nanorod layer and to surface roughness, due to the length distribution of the wires. Importantly, the enhanced transmission measurements of Figure 3a demonstrates that the reduction in specular reflection reported in Figure 3c is not only due to surface roughness or scattering in the nanorod layer, but also to the refractive-index matching that the nanorod layer provides between air and GaP.

Figure 3b, d, and f shows calculations of the transmission and reflection, performed using the thin-film method,[29] of sample I (light-gray dash-dot-dotted curve), sample II (dark-gray dashed curve), and a bare GaP substrate covered on one side with a 500 nm thick SiO_2 layer (black solid curve). The calculated system consists of five layers: air, nanorod layer, GaP substrate, SiO_2, and air. The nanorod layer is considered as sliced into 50 horizontal sublayers, each of which has a thickness of 5 nm. We assume for sample I that the refractive index per sublayer increases quadratically with the length of the nanorods. This quadratic increase is based on the assumption that the filling fraction is proportional to the square of the diameter of the rods, and that the effective refractive index is proportional to the GaP filling fraction. From the calculations, we have determined a variation of the refractive index over the nanorod layer length of sample I from 1.1 up to 2.1. The length distribution of the rods of sample II is determined from SEM images (Fig. 1e). From this length distribution, we can estimate a refractive index profile, which results in a third-order polynomial as a function of depth, in which the refractive index is varied from 1.1 to 1.4 over the nanorod-layer length. The calculations (Fig. 3b, d, and f) show the same trend as the measurements (Fig. 3a, c, and e). The small discrepancies with the measurement can be attributed to the aforementioned scattering, which is not included in the calculations. Both measurement and calculation show a reduction for the sum of transmission and reflection (Fig. 3e and f) with respect to the bare GaP substrate for energies higher than the electronic band gap of GaP. This reduction can be attributed to scattering of light and to an enhanced absorption in GaP due to the antireflection coating. From calculations performed assuming the nanorod layers positioned on top of an infinitely thick GaP substrate (not shown here), we have established that the modulation of the transmission and reflection through samples I and II are due to Fabry–Pérot resonances in the SiO_2 layer at the bottom of the wafer and at the nanorod film on top. This indicates that the nanorod layer acts both as a graded-refractive-index coating and a single-layer interference coating.

In addition to direct transmission and specular reflection measurements, we have performed angle-integrated total reflection and transmission measurements for energies between 0.62 eV ($\lambda = 2000$ nm) and 2.58 eV ($\lambda = 480$ nm), as described in the Experimental section. For these measurements, both the specular or direct light beam and the possibly scattered light are collected using an integrating sphere. Figure 4a shows the total transmission of samples I (light-gray circles) and II (dark-gray triangles) for normal incidence, while Figure 4b displays the total reflection measurement of both samples for an angle of incidence

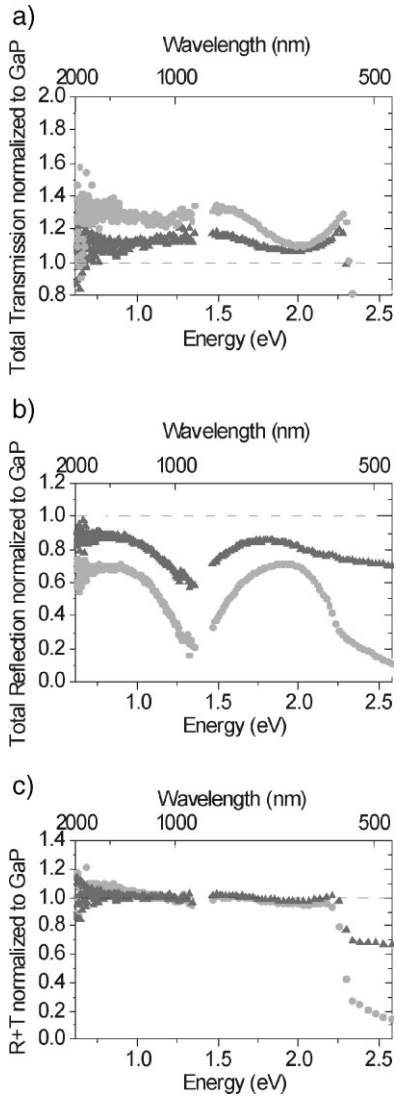

Figure 4. a) Total transmission and b) total reflection of sample I (light-gray circles) and II (dark-gray triangles) normalized to the measurements on a GaP substrate. c) Sums of the total reflection and transmission of samples I (light-gray circles) and II (dark-gray triangles) normalized to the total reflection and transmission of the bare GaP substrate.

of 8° with respect to the normal of the sample. These total transmission and reflection spectra have been normalized by reference measurements of a GaP substrate. The total transmission measurement shows for energies below the electronic band gap, for both samples, an increase with respect to bulk GaP. The overall reduction of the total reflection with respect to the substrate (Fig. 4b) demonstrates that the reduction of the specular reflection of Figure 3c is not due to light scattering in the nanorod film; if the reduction of the specular reflection had been caused by scattering, the angle-integrated total reflection measurement would not show a decreased reflection with respect to the GaP reference, as both scattered light and specular reflection are detected. The dip in normalized reflection at around 1.35 eV ($\lambda = 900$ nm) is caused by the aforementioned combination of a Fabry–Pérot oscillation in the SiO_2 layer at the backside of the GaP

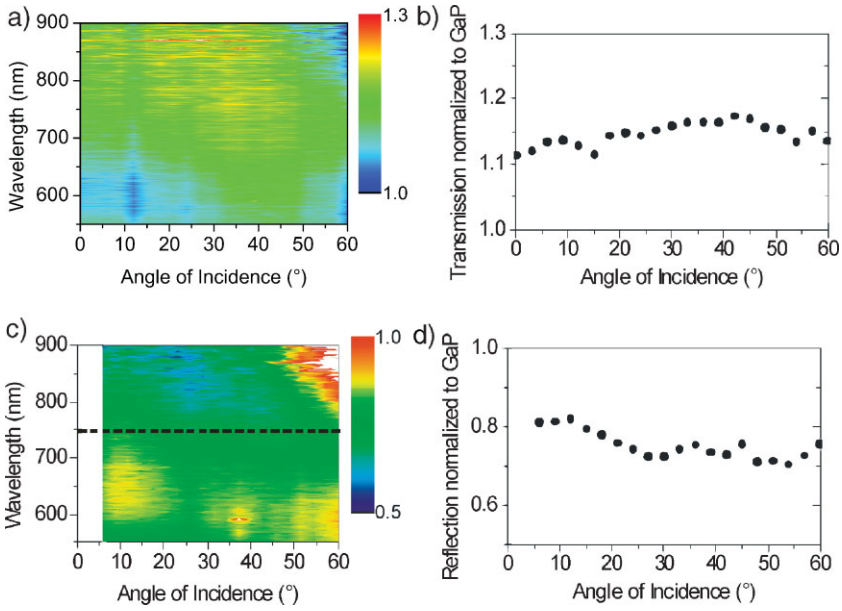

Figure 5. a) Angular-dependent transmission and c) reflection of a layer of GaP nanorods of sample II, normalized to the transmission and reflection of a bare GaP substrate. b,d) Transmission and reflection measurements at 750 nm (along the dotted lines of a) and c)).

substrate and in the nanorod film. As can be seen in Figure 4c, the sum of total transmission and total reflection with respect to the bare GaP substrate is 1 for energies less than 2.26 eV, which shows that there are no absorption losses at these energies. Above the electronic band gap of GaP, there is a reduction of the total transmission plus reflection of the nanorod layer with respect to the bare GaP substrate (see Fig. 4c). This reduction means an enhanced absorption in the nanorod antireflection coating. In summary, these measurements show that layers of nanorods form broad-band antireflection coatings that reduce the total reflection and enhance the total transmission from 2.25 eV ($\lambda = 550$ nm) to at least 0.62 eV ($\lambda = 2000$ nm).

To investigate the omnidirectional characteristics of these antireflection coatings, we have performed direct transmission and specular reflection measurements as a function of wavelength in the range from 550 to 900 nm and for angles of incidence varying from 0 to 60 ° for sample II. This angular range was limited by our experimental setup. Figure 5a shows a contour image of the transmission of the nanorod sample normalized to the transmission of the GaP substrate. For all wavelengths, and at all angles, a transmission exceeding 1 is observed. Figure 5b shows the angle-dependent transmission for a wavelength of 750 nm, taken along the black dotted line in Figure 5a. Figure 5c and d shows the reflection of sample II normalized to the reflection of the GaP reference. The normalized reflection is less than 1 for all wavelengths and in the investigated angular range. Based on these measurements, we conclude that the nanorod layers act as broad-band and omnidirectional antireflection coatings.

In summary, we have investigated the antireflective properties of layers of GaP nanorods using wavelength- and angle-dependent transmission and reflection measurements. The nanorods were fabricated by chemical vapor deposition using the VLS method. We have shown that the enhanced transmission and corresponding reduced reflection of these layers is related to a graded refractive index in the nanorod layer. The enhanced direct transmission and the total transmission and reflection presented in this work show that scattering and absorption are weak in these layers. The antireflection behavior over a broad wavelength and angular range, and the low amount of light scattered, renders these nanorod antireflection coatings a very promising material for enhancing light coupling in solar cells or for more efficient light extraction from LEDs.

Experimental

Growth of Nanorods: Before growth, the (111)A (Ga-terminated) side of the GaP substrate was covered with 500 nm of SiO_2 by plasma-enhanced chemical vapor deposition at a temperature of 300 °C, to protect the backside during the anisotropic etching of the wafer in $HNO_3/HCl/H_2O$ (2:3:3) at 80 °C for 2 min. This etching step is necessary to remove any native oxides that would hinder the nanorod growth. Directly after etching, a thin gold film with a thickness of 0.3 nm was deposited onto the (111)B GaP (P-terminated) substrate side. This gold film acts as a catalyst for the nanorod growth. During annealing, the gold film breaks up into small islands, which form individual catalyst droplets from which the nanorods grow selectively. The gold film of sample I was annealed for 10 min at 570 °C; for sample II this step was left out. The nanorods are grown in the VLS-growth mode in a low-pressure (5×10^3 Pa) metal–organic–vapor phase epitaxy system (Aixtron 200), using trimethylgallium (TMG) and phosphine (PH_3) as precursors, with molar fractions of $\chi_{TMG} = 9.1 \times 10^{-5}$ and $\chi_{PH_3} = 15 \times 10^{-3}$. A total flow of 6 L min^{-1} was used, with hydrogen (H_2) as carrier gas. After growth, the samples were cooled down in a PH_3-containing atmosphere.

Angle-Resolved Specular Reflection and Direct Transmission Measurements: We performed wavelength- and angle-dependent transmission and reflection measurements for wavelengths between 1.38 eV ($\lambda = 900$ nm) and 2.58 eV ($\lambda = 480$ nm) by mounting the sample and detector on a set of computer-controlled rotation stages. The samples were illuminated using a collimated beam of a fiber-coupled halogen lamp (Yokogawa AQ4303), and the spectra were obtained using a spectrometer (Ocean Optics, USB2000).

Angle-Integrated Total Reflection and Transmission Measurements: This measurement was performed using a Lambda 950 spectrometer (PerkinElmer) consisting of a tungsten–halogen and a deuterium lamp and an integrating sphere, in combination with a photomultiplier for visible and a PbS detector for infrared light. For the transmission measurements, the samples were mounted in front of the integrating sphere, so that all the transmitted light was collected. For the reflection measurements, the samples were mounted at the backside of the integrating sphere with an angle of 8 ° with respect to the incident light beam, so that all the reflected light from the sample could be collected and detected.

Acknowledgements

We thank E. Evens and W. van den Einden for technical assistance, H. de Barse and F. Holthuysen for SEM analysis, M. A. Verheijen for TEM analysis, H. Jagt for assistance during the measurements, and P. Johnson for useful discussions. This work is part of the research program of the

''Stichting voor Fundamenteel Onderzoek der Materie (FOM)'', which is financially supported by the ''Nederlandse organisatie voor Wetenschappelijk Onderzoek (NWO)'' and is part of an industrial partnership program between Philips and FOM. For REA the work was carried out under project number MC3.05243 in the framework of the strategic research program of the Materials Innovation Institute (M2i). This article has been amended for print publication.

Received: September 17, 2008
Revised: November 19, 2008
Published online: January 14, 2009

[1] W. H. Southwell, *Opt. Lett.* **1983**, *8*, 584.
[2] J. A. Dobrowolski, D. Poitras, P. Ma, H. Vakil, M. Acree, *Appl. Opt.* **2002**, *41*, 3075.
[3] D. Poitras, J. A. Dobrowolski, *Appl. Opt.* **2004**, *43*, 1286.
[4] T. Lohmüller, M. Helgert, M. Sundermann, R. Brunner, J. P. Spatz, *Nano Lett.* **2008**, *8*, 1429.
[5] Y.-J. Lee, D. S. Ruby, D. W. Peters, B. B. McKenzie, J. W. P. Hsu, *Nano Lett.* **2008**, *8*, 1501.
[6] S. J. An, J. H. Chae, G.-C. Yi, G. H. Park, *Appl. Phys. Lett.* **2008**, *92*, 121108.
[7] J.-Q. Xi, M. F. Schubert, J. K. Kim, E. F. Schubert, M. Chen, S.-Y. Lin, W. Liu, J. A. Smart, *Nat. Photonics* **2007**, *1*, 178.
[8] Y.-F. Huang, S. Chattopadhyay, Y.-J. Jen, C.-Y. Peng, T.-A. Liu, Y.-K. Hsu, C.-L. Pan, H.-C. Lo, C.-H. Hsu, Y.-H. Chang, C.-S. Lee, K.-H. Chen, L.-C. Chen, *Nat. Nanotechnol.* **2007**, *2*, 770.
[9] C. H. Sun, W.-L. Min, N. C. Linn, P. Jiang, B. Jiang, *Appl. Phys. Lett.* **2007**, *91*, 231105.
[10] C. H. Sun, P. Jiang, B. Jiang, *Appl. Phys. Lett.* **2008**, *92*, 061112.
[11] Z. Yu, H. Gao, W. Wu, H. Ge, S. Y. Ghou, *J. Vac. Sci. Technol, B* **2003**, *21*, 2874.
[12] Z. P. Yang, L. C. Ci, J. A. Bur, S. Y. Lin, P. M. Ajayan, *Nano Lett.* **2008**, *8*, 446.
[13] F. J. Garcia-Vidal, *Nat. Photonics* **2008**, *2*, 215.
[14] C. H. Chiu, P. Yu, H. C. Kuo, C. C. Chen, T. C. Lu, S. C. Wang, S. H. Hsu, Y. J. Cheng, Y. C. Chang, *Opt. Express* **2008**, *16*, 8748.
[15] J. A. Dobrowolski, in *Handbook of Optics*, Vol. *1*(Eds: M. Bass, E. W. van Stryl, D. R. Williams, W. L. Wolfe), McGraw-Hill, Inc., New York **1995**, Ch. 42.
[16] D. S. Hobbs, B. D. Macleod, J. R. Riccobono, *Proc. SPIE.* **2007**, *6545*, 65450y.
[17] C. G. Bernhard, *Endeavour* **1967**, *26*, 79.
[18] D. G. Stavenga, S. Foletti, G. Palasantzas, K. Arikawa, *Proc. R. Soc. B* **2006**, *273*, 661.
[19] R. S. Wagner, W. C. Ellis, *Appl. Phys. Lett.* **1964**, *4*, 89.
[20] L. J. Lauhon, M. S. Gudiksen, D. Wang, C. M. Lieber, *Nature* **2002**, *420*, 57.
[21] J. B. Hannon, S. Kodambaka, F. M. Ross, R. M. Tromp, *Nature* **2006**, *440*, 69.
[22] M. T. Borgström, G. Immink, B. Ketelaars, R. Algra, E. P. A. M. Bakkers, *Nat. Nanotechnol.* **2007**, *2*, 541.
[23] M. T. Björk, B. J. Ohlsson, T. Sass, A. I. Persson, C. Thelander, M. H. Magnusson, K. Deppert, L. R. Wallenberg, L. Samuelson, *Nano Lett.* **2002**, *2*, 87.
[24] M. H. Huang, S. Mao, H. Feick, H. Yan, Y. Wu, H. Kind, E. Weber, R. Russo, P. Yang, *Science* **2001**, *292*, 1897.
[25] K. Hiruma, M. Yazawa, T. Katsuyama, K. Ogawa, K. Haraguchi, M. Koguchi, H. Kakibayashi, *J. Appl. Phys.* **1995**, *77*, 447.
[26] M. A. Verheijen, G. Immink, T. de Smet, M. T. Borgström, E. P. A. M. Bakkers, *J. Am. Chem. Soc.* **2006**, *128*, 1353.
[27] O. L. Muskens, S. L. Diedenhofen, M. H. M. Van Weert, M. T. Borgström, E. P. A. M. Bakkers, J. Gómez Rivas, *Adv. Funct. Mater.* **2008**, *18*, 1039.
[28] O. L. Muskens, M. T. Borgström, E. P. A. M. Bakkers, J. Gómez Rivas, *Appl. Phys. Lett.* **2006**, *89*, 233117.
[29] P. Yeh, *Optical Waves in Layered Media*, John Wiley and Sons, New York, Chichester, Brisbane, Toronto, Singapore **1948**, Ch. 6.